Supplement of Atmos. Chem. Phys., 23, 7521–7534, 2023
https://doi.org/10.5194/acp-23-7521-2023-supplement

Atmospheric Chemistry and Physics
Open Access

Supplement of

The variation in the particle number size distribution during the rainfall: wet scavenging and air mass changing

Guangdong Niu et al.

Correspondence to: Ximeng Qi (qiximeng@nju.edu.cn)

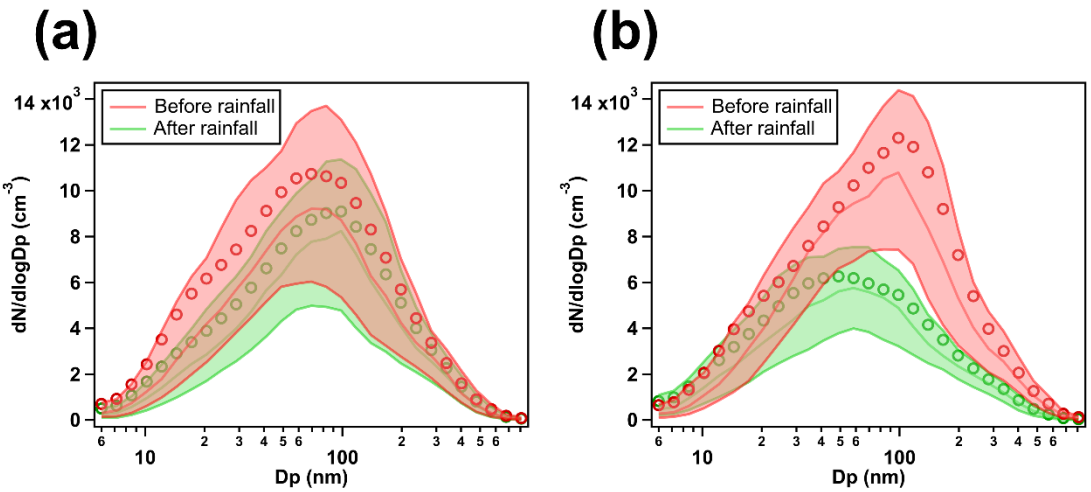

Figure S1. The PNSD before and after rainfall events for (a) normal scavenging events and (b) high-BWSC events. The lines represent the median, 25th and 75th percentiles and the circles represent the average.

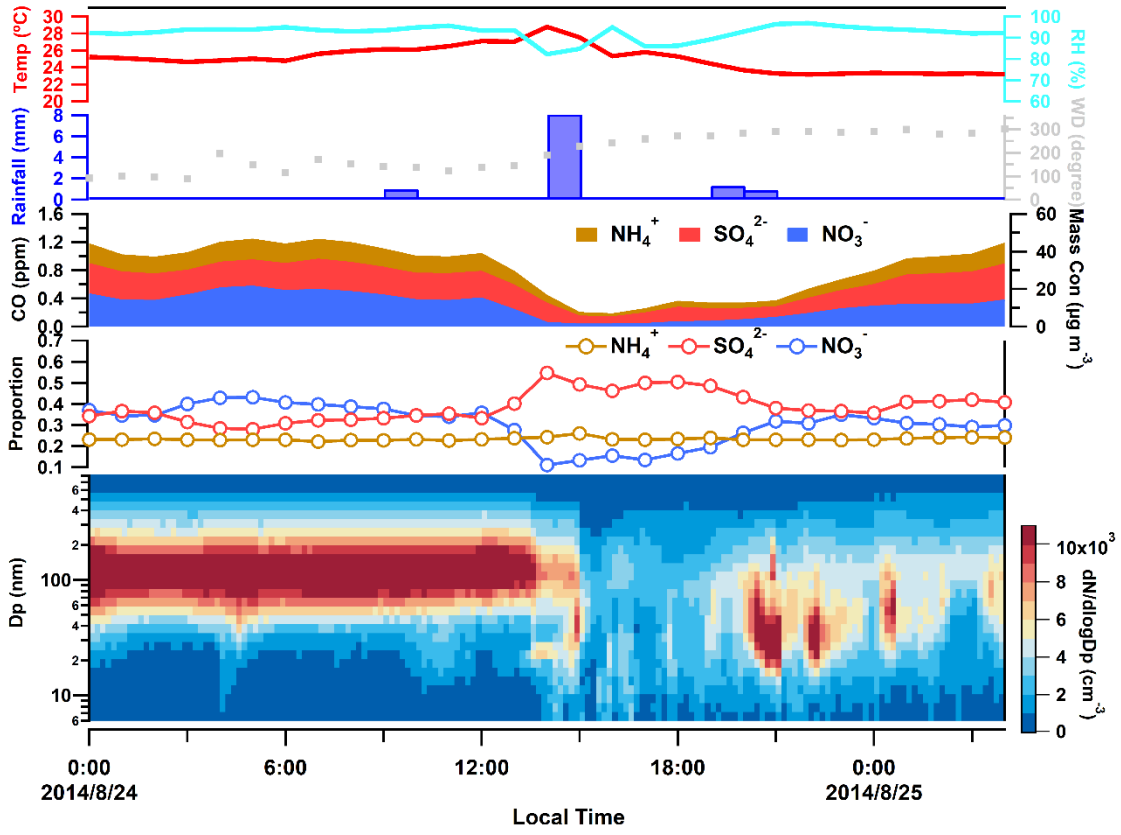

Figure S2. **Typical case for type i high-BWSC event**. Top to bottom panels are time series of ambient temperature, RH (relative humidity), precipitation, wind direction, SNA (sulfate, nitrate, ammonium) concentrations, fractions of SNA in water soluble ions (WSIs), and particle number size distribution in Nanjing on 24-25 August 2014.

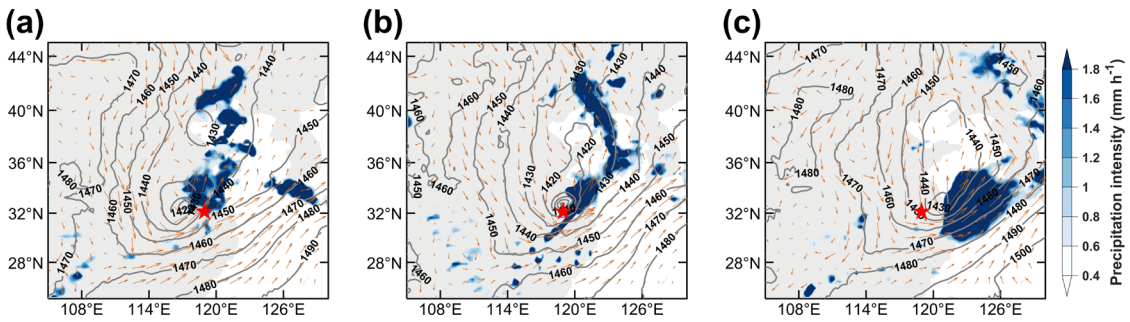

Figure S3. **Typical case for type i high-BWSC event**. Distributions of winds and geopotential heights at 850 hPa and precipitation intensity (a) before, (b) at and (c) after the moment of sudden decrease in particle number concentration for the typical type i high-BWSC event (24-25 August 2014) in Nanjing. The red pentagram shows the location of SORPES.

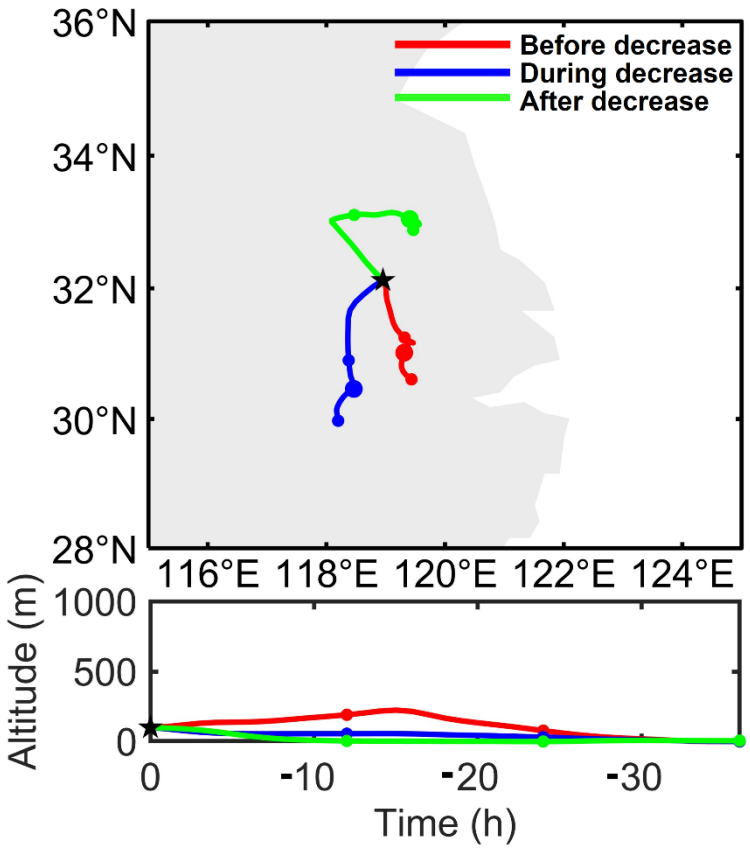

Figure S4. **Typical case for type i high-BWSC event**. The backward trajectories of air masses before, at and after the moment of sudden decrease in particle number concentration for the typical type i high-BWSC event (24-25 August 2014) in Nanjing. The black pentagram shows the location of SORPES.

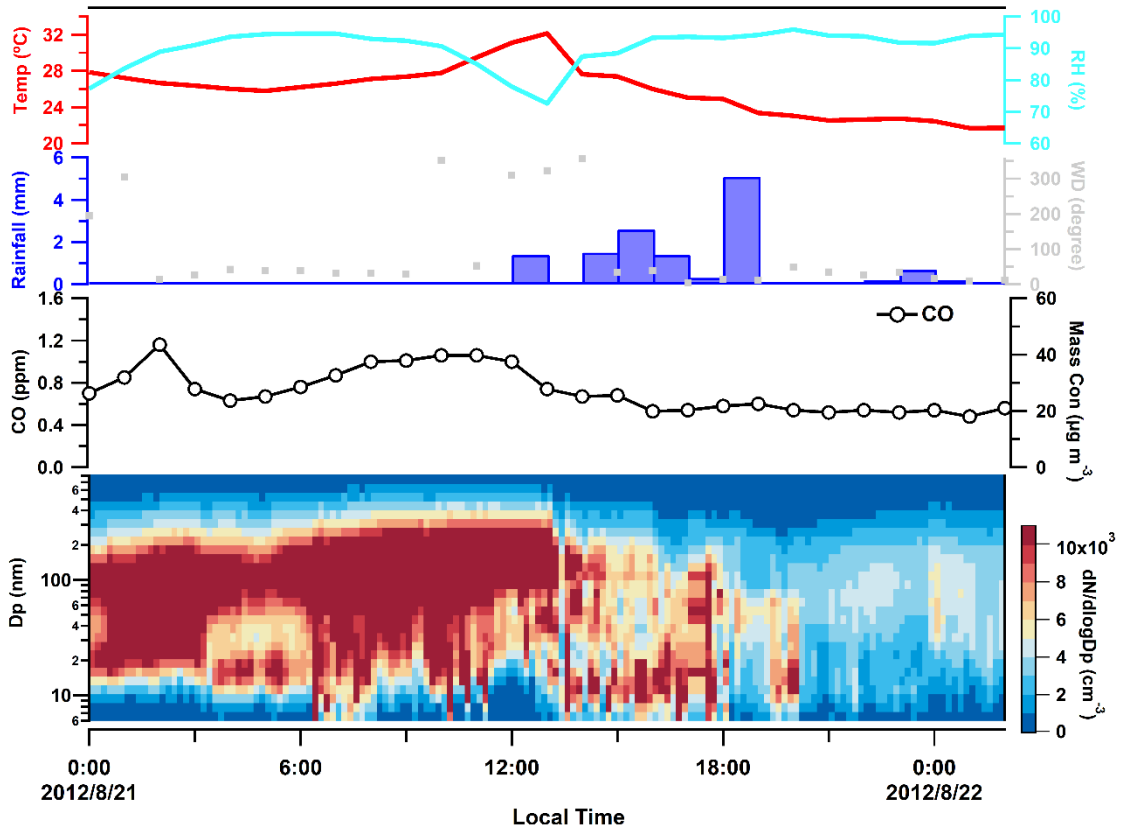

Figure S5. **Typical case for type ii high-BWSC event**. Top to bottom panels are time series of ambient temperature, RH, precipitation, wind direction, CO concentration, and particle number size distribution in Nanjing on 21-22 August 2012.

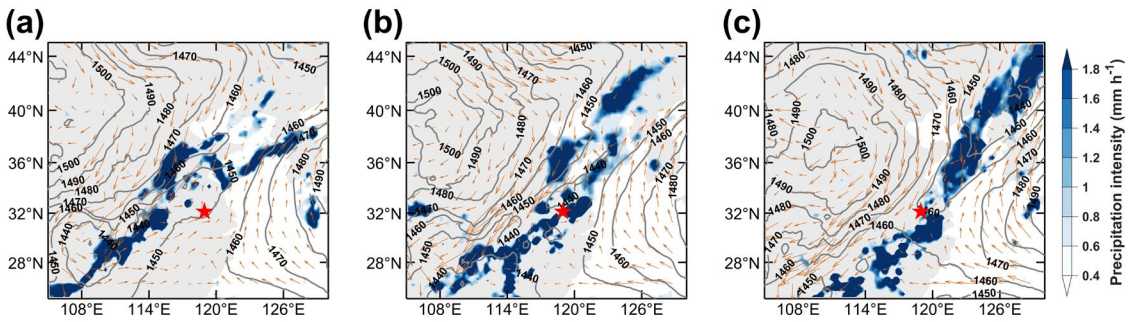

Figure S6. **Typical case for type ii high-BWSC event.** Distributions of winds and geopotential heights at 850 hPa and precipitation intensity (a) before, (b) at and (c) after the moment of sudden decrease in particle number concentration for the typical type ii high-BWSC event (21-22 August 2012) in Nanjing. The red pentagram shows the location of SORPES.

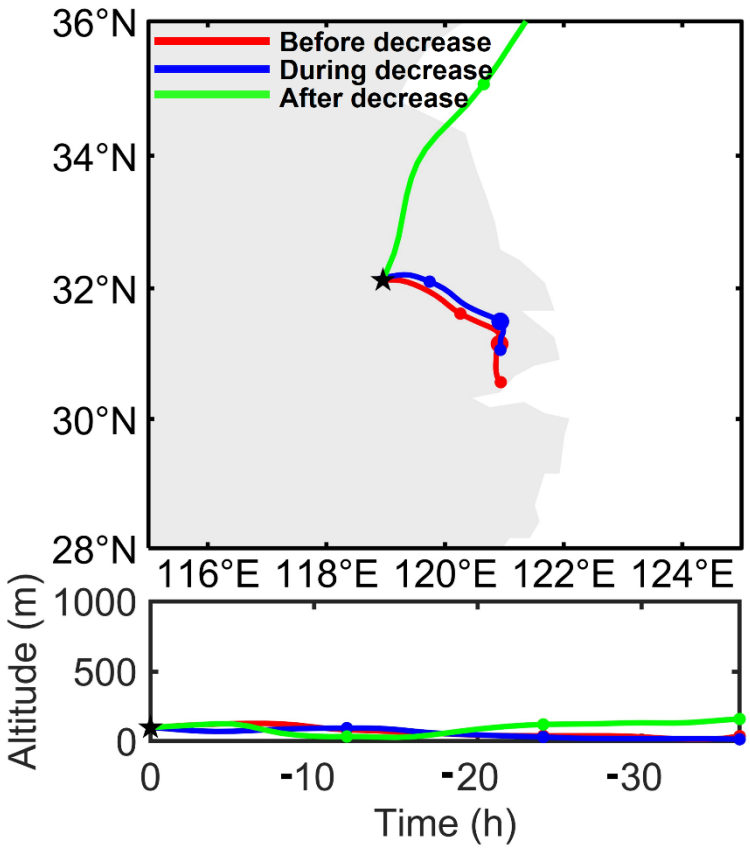

Figure S7. **Typical case for type ii high-BWSC event**. The backward trajectories of air masses before, at and after the moment of sudden decrease in particle number concentration for the typical type ii high-BWSC event (21-22 August 2012) in Nanjing. The black pentagram shows the location of SORPES.

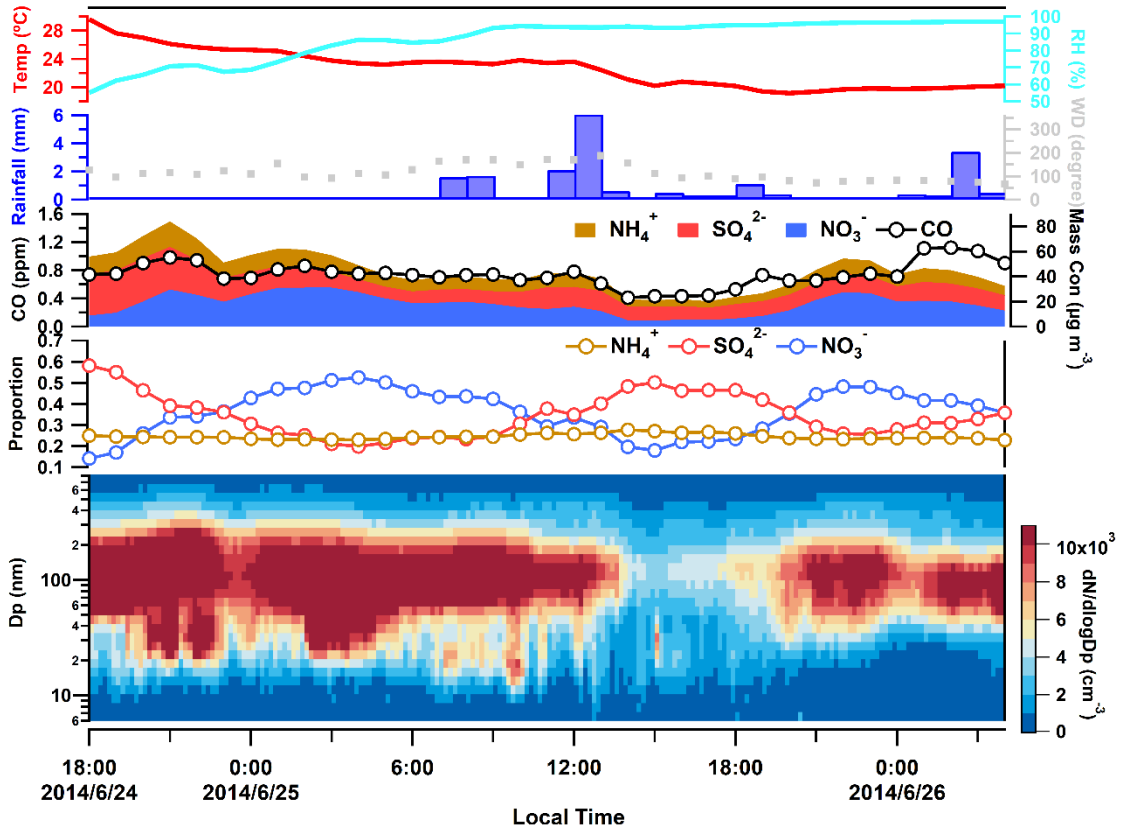

Figure S8. **Typical case for type iii high-BWSC event**. Top to bottom panels are time series of ambient temperature, RH, precipitation, wind direction, CO concentration, SNA (sulfate, nitrate, ammonium) concentrations, fractions of SNA in WSIs, and particle number size distribution in Nanjing on 24-26 June 2014.

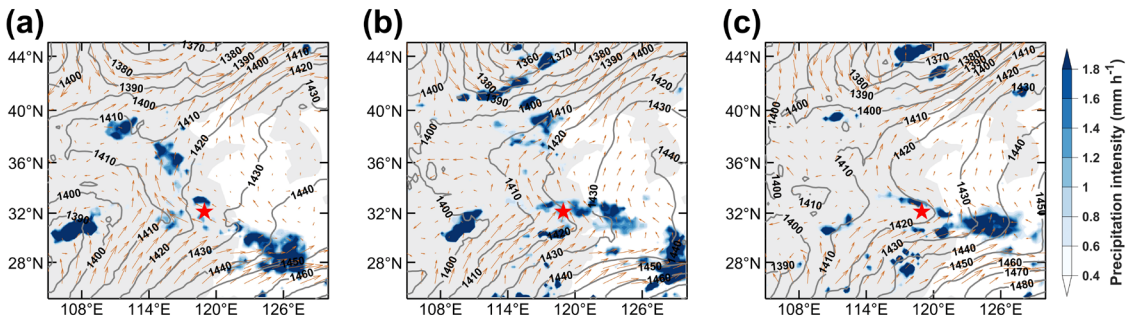

Figure S9. **Typical case for type iii high-BWSC event.** Distributions of winds and geopotential heights at 850 hPa and precipitation intensity (a) before, (b) at and (c) after the moment of sudden decrease in particle number concentration for the typical type iii high-BWSC event (24-26 June 2014) in Nanjing. The red pentagram shows the location of SORPES.

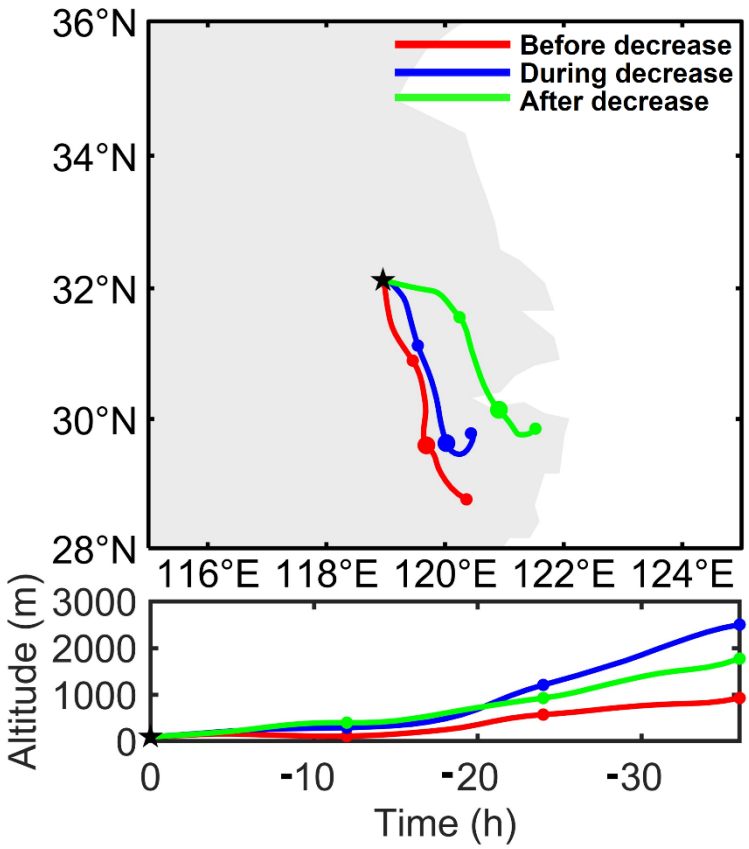

Figure S10. **Typical case for type iii high-BWSC event.** The backward trajectories of air masses before, at and after the moment of sudden decrease in particle number concentration for the typical type iii high-BWSC event (24-26 June 2014) in Nanjing. The black pentagram shows the location of SORPES.

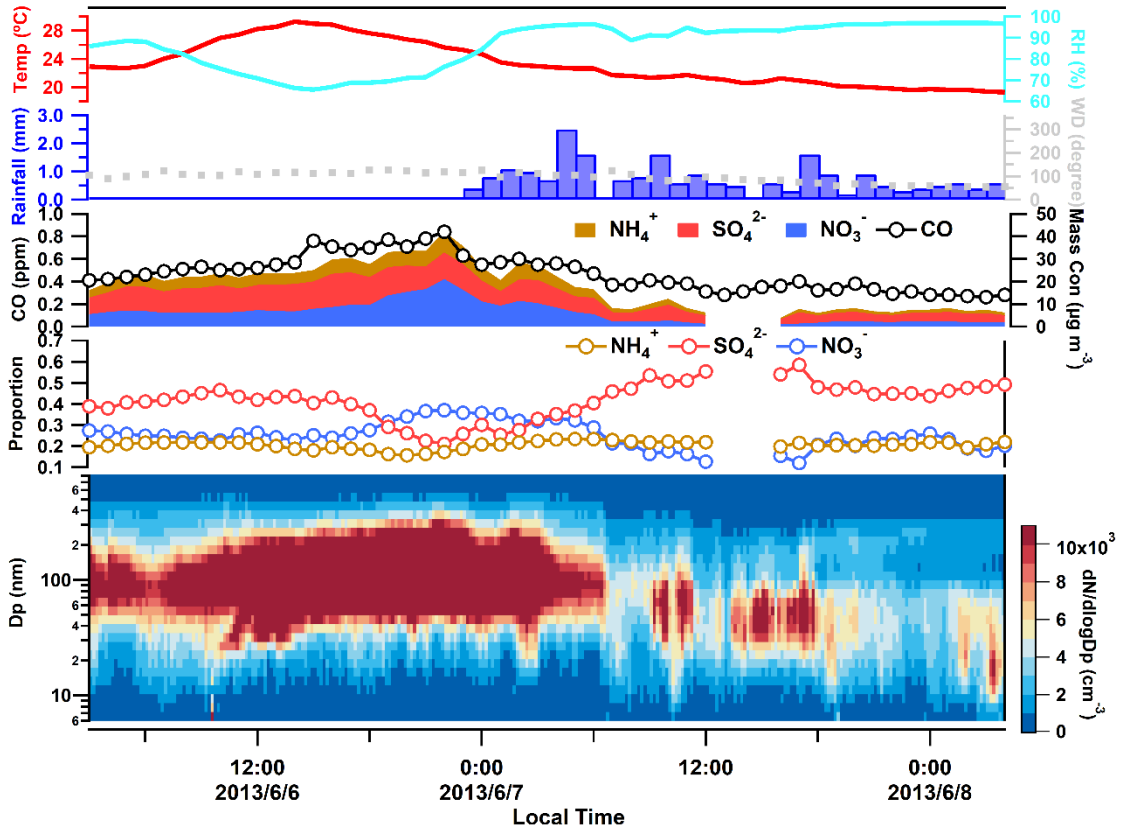

Figure S11. **Typical case for type iv high-BWSC event**. Top to bottom panels are time series of ambient temperature, RH, precipitation, wind direction, CO concentration, SNA (sulfate, nitrate, ammonium) concentrations, fractions of SNA in WSIs, and particle number size distribution in Nanjing on 6-8 June 2013.

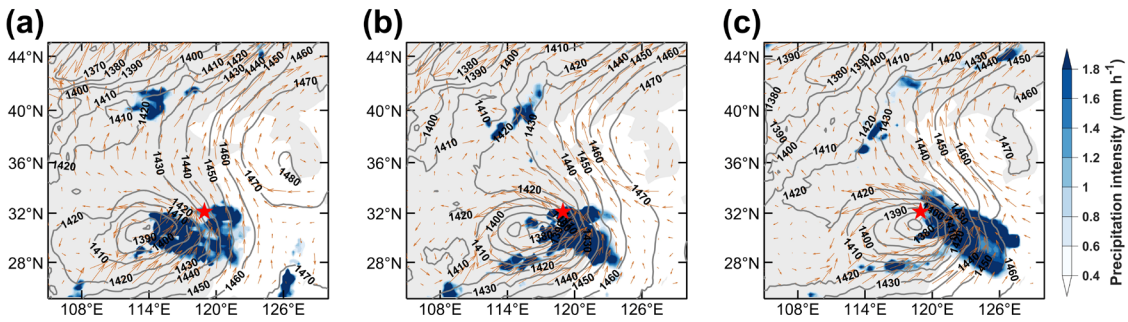

Figure S12. **Typical case for type iv high-BWSC event**. Distributions of winds and geopotential heights at 850 hPa and precipitation intensity (a) before, (b) at and (c) after the moment of sudden decrease in particle number concentration for the typical type iv high-BWSC event (6-8 June 2013) in Nanjing. The red pentagram shows the location of SORPES.

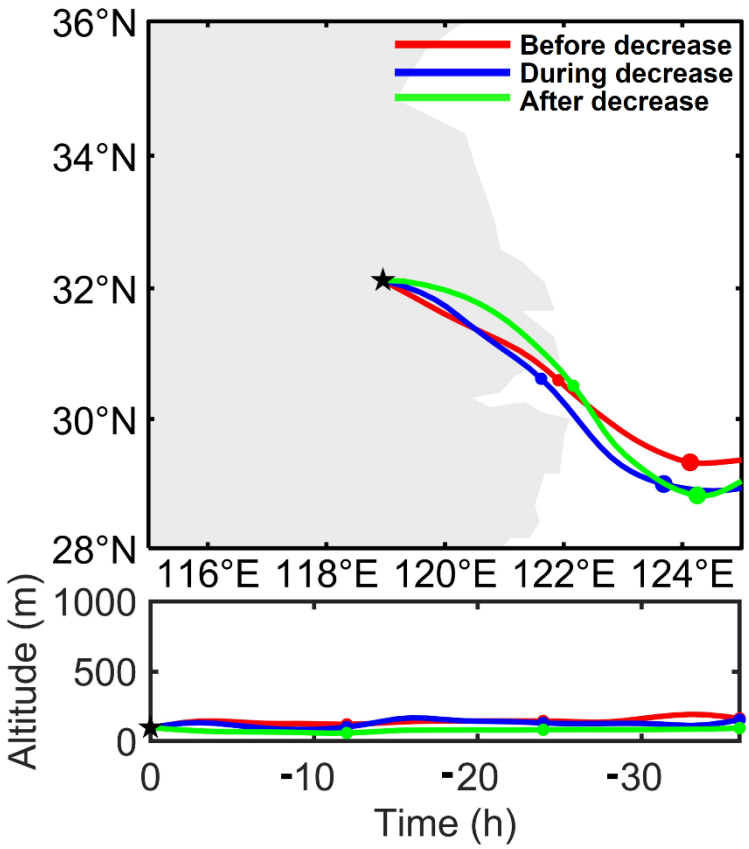

125

Figure S13. **Typical case for type iv high-BWSC event.** The backward trajectories of air masses before, at and after the moment of sudden decrease in particle number concentration for the typical type iv high-BWSC event (6-8 June 2013) in Nanjing. The black pentagram shows the location of SORPES.

130

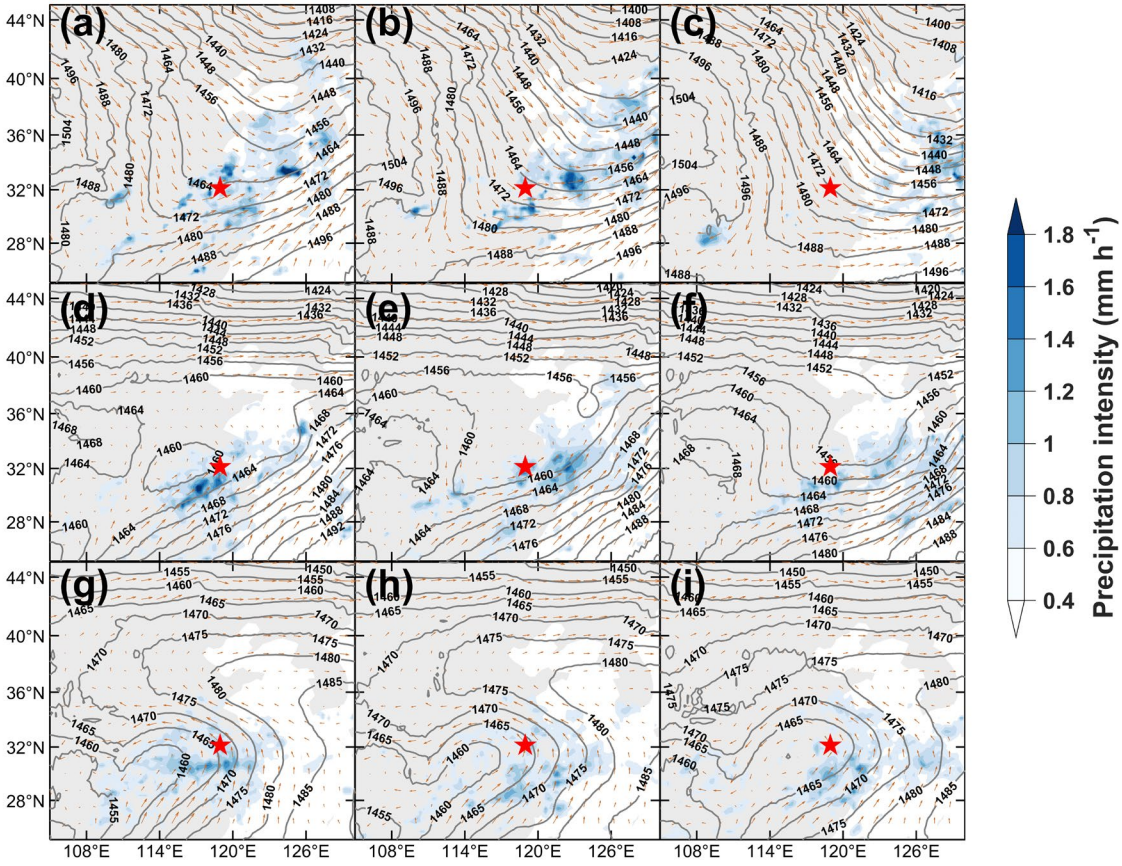

Figure S14. **Synoptic situations for normal scavenging events.** Distributions of winds and geopotential heights at 850 hPa and precipitation intensity before, during and after the rainfall events for (a-c) trough type, (d-f) vortex-weakening type, and (g-i) vortex type of normal scavenging events. The red pentagram shows the location of SORPES.

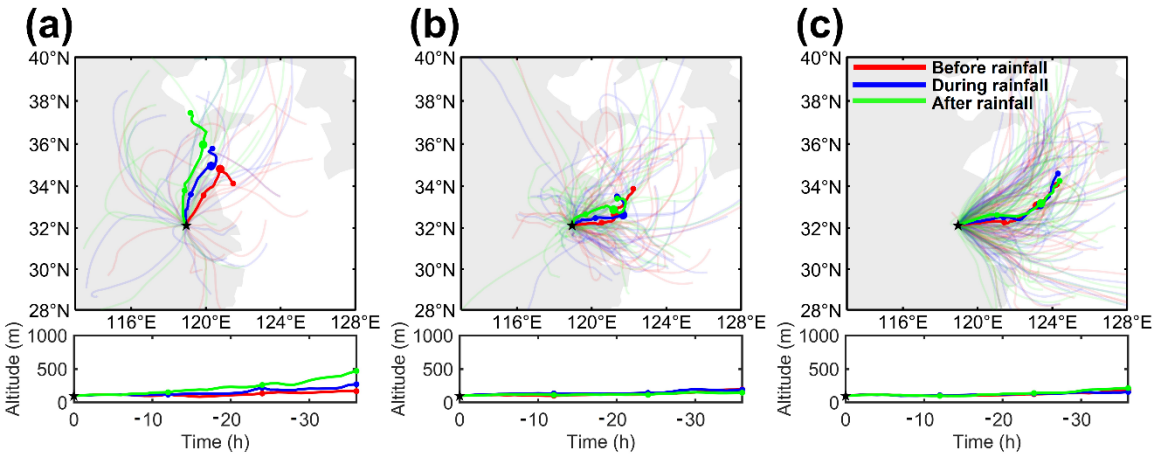

Figure S15. **Backward trajectories of air masses for normal scavenging events.** The backward trajectories of air masses before, during and after the rainfall events for (a) trough type, (b) vortex-weakening type, and (c) vortex type of normal scavenging events. The black pentagram shows the location of SORPES.

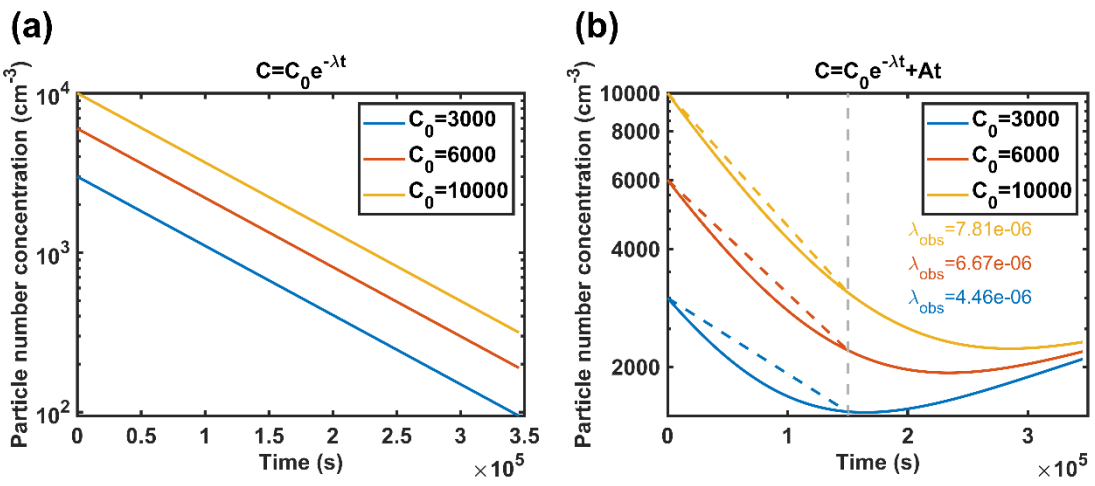

Figure S16. The variation of particle number concentration with time during rainfall under theoretical conditions (a) without and (b) with the stable source. (Assuming the scavenging coefficient (λ) of 1×10^{-5} s^{-1} and the particle formation rate (A) of 5.8×10^{-3} cm^{-3} s^{-1})